ARID ZONE JOURNAL OF ENGINEERING, TECHNOLOGY & ENVIRONMENT
AZOJETE June 2026. Vol.22(2):351-365
Published by the Faculty of Engineering, University of Maiduguri, Maiduguri, Nigeria.
Print ISSN: 1596-2490, Electronic ISSN: 2545-5818
https://doi.org/10.63958/AZOJETE/2026/22/02/013
www.azojete.com.ng

ORIGINAL RESEARCH ARTICLE

A RECURSIVE LEAST SQUARES-BASED ADAPTIVE FUZZY LOGIC APPROACH FOR HIGH-PERFORMANCE MAXIMUM POWER POINT TRACKING IN PHOTOVOLTAIC SYSTEMS

B. O. Akinloye* and A. Suleiman

Department of Electrical and Electronics Engineering, Federal University of Petroleum Resources, Warri, Nigeria
**Corresponding author's email: akinloyebenolabisi@gmail.com*

ARTICLE INFORMATION

Received: 6th March 2026
Revised: 21st March 2026
Accepted: 2nd April 2026

Keywords:
Adaptive fuzzy logic control
Maximum power point tracking
Photovoltaic systems
Recursive least squares
Solar

ABSTRACT

The growing demand for high-efficiency renewable energy systems has intensified research into advanced photovoltaic (PV) energy optimization techniques. Maximum Power Point Tracking (MPPT) is essential for maximizing energy extraction from PV systems under varying environmental conditions. Among the available techniques, intelligent control strategies such as Fuzzy Logic Control (FLC) and Adaptive Fuzzy Logic Control (AFLC) have attracted considerable attention due to their robustness and adaptability. However, conventional methods, including standard FLC, often suffer from reduced tracking accuracy, slower dynamic response, and increased steady-state oscillations under rapidly changing irradiance and temperature conditions—challenges that are particularly pronounced in tropical environments with frequent atmospheric fluctuations. This study presents the design and simulation of an Adaptive Fuzzy Logic Controller (AFLC) based MPPT system for a PV array integrated with a DC–DC boost converter. The system is modeled in MATLAB/Simulink, where both FLC and AFLC techniques are implemented and evaluated under varying environmental conditions. The proposed AFLC enhances performance by dynamically adjusting its membership functions, scaling factors, and rule weights in real time using Recursive Least Squares (RLS) adaptation. It was observed that Simulation results of the AFLC significantly outperforms the conventional FLC approach. The AFLC achieves a tracking efficiency of 91.36%, representing a 5.78% improvement over FLC. The response time is reduced by 90.9% (from 0.11 s to 0.01 s), while oscillations around the Maximum Power Point (MPP) are decreased by 68.9% (from 18.5% to 5.76%). Furthermore, under partial shading conditions, the AFLC effectively avoids local maxima and extracts up to 15% more power. Overall, the proposed AFLC-based MPPT system offers superior tracking speed, accuracy, and stability, making it a highly effective solution for enhancing PV system performance in dynamic and real-world operating conditions.

1.0 Introduction

The global transition to renewable energy has positioned photovoltaic (PV) systems as a cornerstone for sustainable power generation (IEC, 2023). With increasing solar penetration in grids worldwide, maximizing energy harvest from PV installations has become critical (Mellit and Kalogirou, 2014). PV power output primarily depends on solar irradiance and cell temperature, both exhibiting significant temporal and spatial variations (Esram and Chapman, 2007). System efficiency is highest at the Maximum Power Point (MPP), where the voltage-current product peaks (Liu *et al.*, 2008), but the MPP shifts continuously with environmental changes, requiring advanced tracking strategies (Ishaque and Salam, 2013). This challenge is

acute in tropical climates like Nigeria, where rapid weather fluctuations, cloud-induced partial shading, and seasonal variations create highly dynamic conditions (Salas *et al*., 2006).

Conventional Maximum Power Point Tracking (MPPT) techniques, such as Perturb and Observe (P&O) and Incremental Conductance, are widely used due to their simplicity (Elgendy *et al*., 2012). The P&O method perturbs operating voltage and adjusts based on power changes (Al-Diab and Sourkounis, 2010). However, in dynamic environments, these methods suffer from oscillations around the MPP causing energy losses (Kamarzaman and Tan, 2014), slow response to rapid irradiance changes due to fixed step sizes (Messalti *et al*., 2017), failure to escape local maxima under partial shading (Mohamed and El-Sayed, 2018) and sensitivity to sensor noise (Nabipour *et al*., 2017).

To overcome these limitations, artificial intelligence-based approaches, including neural networks, genetic algorithms, and fuzzy logic control, have gained attention (Reisi *et al*., 2013). Fuzzy Logic Control (FLC) is particularly effective, handling nonlinearities and uncertainties without precise mathematical models through linguistic rules and membership functions (Alajmi *et al*., 2011). Nevertheless, traditional FLC relies on fixed rule bases and membership functions, limiting its adaptability to rapid or significant environmental changes (Larbes *et al*., 2009).

Adaptive Fuzzy Logic Control (AFLC) addresses these drawbacks by dynamically adjusting parameters such as membership functions, rule bases, and scaling factors in real-time (Aouchiche *et al*., 2018), enabling robust tracking accuracy and stability under fluctuating conditions (Ahmed *et al*., 2015). Building on this capability, this research develops a comprehensive AFLC framework for Maximum Power Point Tracking (MPPT) in photovoltaic systems. The proposed approach incorporates Recursive Least Squares (RLS) for real-time parameter tuning and implements dynamic adjustment of membership functions to enhance system responsiveness. The performance of the developed controller is thoroughly evaluated under standard test conditions, rapid irradiance variations, and partial shading scenarios. In addition, a quantitative comparison with conventional Fuzzy Logic Control (FLC) is conducted, demonstrating improvements in tracking efficiency, response time, and overall system stability.

2. Materials and Methods

2.1 PV Cell Mathematical Model

Accurate modeling of PV cell behavior is fundamental to MPPT design and validation. The single-diode model, which provides an effective balance between computational complexity and accuracy (Ishaque and Sala, 2013), is employed in this research. The model comprises a photocurrent source (I_{ph}), a diode representing the p-n junction, series resistance (R_s), and shunt resistance (R_{sh}).

The current-voltage relationship for a PV cell is described by Equation 1.

$$I = I_{ph} - I_s\left[\exp\left(\frac{V+IR_s}{V_t}\right) - 1\right] - \frac{V+IR_s}{R_{sh}} \quad (1)$$

where: I = cell current (A), V = cell voltage (V), I_{ph} = photocurrent (A), I_s = diode saturation current (A), R_s = series resistance (Ω), R_{sh} = shunt resistance (Ω), V_t = thermal voltage (V)

The photocurrent in Equation 2, is directly proportional to solar irradiance and is also influenced by cell temperature.

$$I_{ph} = \frac{G}{G_{ref}}\left[I_{ph,ref} + \alpha_{Isc}(T - T_{ref})\right] \quad (2)$$

where: G = solar irradiance (W/m²), G_{ref} = reference irradiance (1000 W/m²), T = cell temperature (K), T_{ref} = reference temperature (298.15 K), α_{Isc} = short-circuit current temperature coefficient

The diode saturation current varies with temperature given by Equation 3.

$$I_s(T) = I_s(T_0)\left(\frac{T}{T_0}\right)^3 \exp\left[\frac{E_g}{k}\left(\frac{1}{T_0} - \frac{1}{T}\right)\right] \quad (3)$$

where: E_g = band gap energy of silicon (1.11 eV), k = Boltzmann constant (8.617 × 10^{-5} eV/K). The thermal voltage is given by Equation 4.

$$V_t = \frac{nkT}{q} \quad (4)$$

where: n = diode ideality factor (typically 1.0-1.5), q = elementary charge (1.602 × 10^{-19} C)

Corresponding author's email address: akinloyebenolabisi@gmail.com

2.2 PV Module and Array Configuration

PV modules are constructed by connecting multiple PV cells in series and parallel configurations to achieve desired voltage and current ratings. For a module with N_s cells in series and N_p cells in parallel, the output voltage and current are given by Equation 5 and 6.

$$V_{module} = N_s \times V_{cell} \quad (5)$$

$$I_{module} = N_p \times I_{cell} \quad (6)$$

Similarly, the PV array output is formed using Equation 7 and 8.

$$V_{array} = N_{ms} \times V_{module} \quad (7)$$

$$I_{array} = N_{mp} \times I_{module} \quad (8)$$

where N_{ms} and N_{mp} represent the number of modules in series and parallel, respectively.

Table 1 summarizes the key parameters of the PV system utilized in this study. The values presented are representative examples generated for simulation purposes.

Table 1: PV Module and Array Specifications

Parameter	Symbol	Value	Unit
Open-circuit voltage	V_{oc}	22	V
Short-circuit current	I_{sc}	5	A
Voltage at MPP	V_{mpp}	18	V
Current at MPP	I_{mpp}	4.5	A
Maximum power	P_{mpp}	81	W
Number of series cells	N_s	36	-
Number of parallel cells	N_p	1	-
Series modules per string	N_{ms}	5	-
Parallel strings	N_{mp}	3	-
Array maximum power	P_{array}	1215	W

2.3 DC-DC Boost Converter

For MPPT implementation, a DC-DC boost converter is employed to interface the PV array with the load. The voltage gain relationship is shown in Equation 9.

$$\frac{V_{out}}{V_{in}} = \frac{1}{1-D} \quad (9)$$

where D is the duty cycle (0 < D < 1).

System specifications for the converter, assuming a 50kHz switching frequency and a 48V battery load, are calculated in Equations 10 through 14.

Required Duty Cycle:

$$D = 1 - \frac{V_{in}}{V_{out}} = 1 - \frac{18}{48} = 0.625 \quad (10)$$

Inductor Selection (for CCM):

$$L_{min} = \frac{V_{in}D}{\Delta I_L f_s} = \frac{V_{mpp}D}{\Delta I_L f_s} \quad (11)$$

Assume $\Delta I_L = 10\% I_{in} = 0.5A$, $f_s = 50\ kHz$

$$L_{min} = \frac{18\ x\ 0.625}{0.5\ x\ 50{,}000} = 450\mu H\ (Use\ L = 1mH) \quad (12)$$

Capacitor Selection (for <1% ripple):

$$C = \frac{I_{out}D}{\Delta V_{out} f_s} \quad (13)$$

Assume $\Delta V_{out} = 0.5V$, $I_{out} = \frac{81W}{48V} \approx 1.6875A$

$$C = \frac{1.6875\ x\ 0.625}{0.5\ x\ 50{,}000} \approx 42uF\ (Use\ C = 100\mu F) \quad (14)$$

The inductor current in continuous conduction mode (CCM) is shown in Equation 15:

Corresponding author's email address: akinloyebenolabisi@gmail.com

$$I_L = \frac{I_{out}}{1-D} \quad (15)$$

The state-space model of the boost converter is described by Equation 16 and 17:

$$\frac{di_L}{dt} = \frac{V_{in}-(1-D)V_{out}}{L} \quad (16)$$

$$\frac{dv_C}{dt} = \frac{(1-D)i_L-I_{load}}{C} \quad (17)$$

2.4 Maximum Power Point Tracking Principles

The MPPT algorithm's objective is to maintain operation at the point where power is maximized despite environmental variations (Said *et al*., 2015).

The tracking efficiency is given in Equation 18:

$$\eta_{MPPT} = \frac{P_{actual}}{P_{mpp}} \times 100\% \quad (18)$$

where: P_{actual} = average power harvested during operation, P_{mpp} = theoretical maximum available power

2.5 Adaptive Fuzzy Logic Controller Design

2.5.1 Input variables

The AFLC employs two input variables to determine the appropriate control action:

i. **Error (E):** Represents the deviation from the MPP, calculated using Equation 19:

$$E(k) = \frac{P(k)-P(k-1)}{V(k)-V(k-1)} \approx \frac{dP}{dV} \quad (19)$$

where $P(k)$ and $V(k)$ are the instantaneous power and voltage at sampling instant k respectively

ii. **Change in Error (ΔE):** Indicates the rate of change of error and it is obtained using Equation 20:

$$\Delta E(k) = E(k) - E(k-1) \quad (20)$$

These variables provide information about both the distance from MPP and the direction of movement toward or away from the optimal operating point.

2.5.2 Fuzzification and membership functions

Inputs are normalized using adaptive scaling factors as shown in Equations 21 and 22:

$$E_{scaled} = \frac{E}{K_E \times G} \quad (21)$$

$$\Delta E_{scaled} = \frac{\Delta E}{K_{\Delta E} \times T} \quad (22)$$

where: K_E, $K_{\Delta E}$ = adaptive gains, G = solar irradiance (W/m²), T = temperature (°C)

The membership functions for Error (E) are defined with five linguistic variables:

i. NL (Negative Large): [-1, -0.5, 0]
ii. NS (Negative Small): [-0.5, -0.1, 0]
iii. Z (Zero): [-0.1, 0, 0.1]
iv. PS (Positive Small): [0, 0.1, 0.5]
v. PL (Positive Large): [0.5, 1, 1]

Corresponding author's email address: akinloyebenolabisi@gmail.com

For Change in Error (ΔE), three membership functions are used:

i. N (Negative): [-0.2, -0.1, 0]
ii. Z (Zero): [-0.05, 0, 0.05]
iii. P (Positive): [0, 0.1, 0.2]

2.5.3 Rule base

The rule base is derived from the sign and magnitude of $\frac{dP}{dV}$, which determines the direction of movement toward the MPP. Large deviations require aggressive duty cycle changes, while small deviations require fine adjustments. The complete rule base is presented in Table 2.

Table 2: Fuzzy Rule Base For MPPT

E \ ΔE	N	Z	P
NL	PL	PL	PS
NS	PL	PS	Z
Z	PS	Z	NS
PS	Z	NS	NL
PL	NS	NL	NL

The output variable is the duty cycle adjustment (ΔD), with membership functions:

i. **NL (Negative Large):** Decrease duty cycle significantly
ii. **NS (Negative Small):** Decrease duty cycle slightly
iii. **Z (Zero):** Maintain current duty cycle
iv. **PS (Positive Small):** Increase duty cycle slightly
v. **PL (Positive Large):** Increase duty cycle significantly

2.5.4 Defuzzification

The centroid method is employed and is given in Equation 23:

$$\Delta D = \frac{\sum_{i=1}^{n} \mu_i \times c_i}{\sum_{i=1}^{n} \mu_i} \quad 23$$

where: μ_i = membership degree of output fuzzy set, i - c_i = centroid of output fuzzy set, i - n = number of output fuzzy sets

2.5.5 Adaptive mechanisms

The distinguishing feature of the AFLC is its ability to adapt parameters in real-time. Three adaptation mechanisms are implemented:

i. **Adaptive Membership Functions:** The shape and position of MFs are adjusted using Recursive Least Squares (RLS) algorithm. The RLS update are given in Equations 24, 25 and 26:

$$\theta(k) = \theta(k-1) + K(k)[y(k) - \phi^T(k)\theta(k-1)] \quad 24$$

$$K(k) = \frac{P(k-1)\phi(k)}{\lambda + \phi^T(k)P(k-1)\phi(k)} \quad 25$$

$$P(k) = \frac{1}{\lambda}[P(k-1) - K(k)\phi^T(k)P(k-1)] \quad 26$$

where: θ = parameter vector (MF centers and widths), λ = forgetting factor (0.97 in this study), K = Kalman gain, P = covariance matrix, ϕ = regression vector

ii. **Adaptive Scaling Factors:** The output scaling factor is dynamically adjusted based on error magnitude, shown in Equation 27:

Corresponding author's email address: akinloyebenolabisi@gmail.com

$$\Delta D_{adapted} = \Delta D_{base} \times \left(1 - e^{-|E|}\right) \quad 27$$

This ensures aggressive tracking (large steps) when far from MPP and fine-tuning (small steps) when near MPP.

iii. **Rule Weight Adaptation:** Rule weights are periodically updated using Particle Swarm Optimization (PSO) to optimize transient and steady-state performance. Rules emphasizing rapid response are prioritized during large error conditions, while fine-tuning rules are favored near MPP.

The overall system configuration is illustrated in Figure 1.

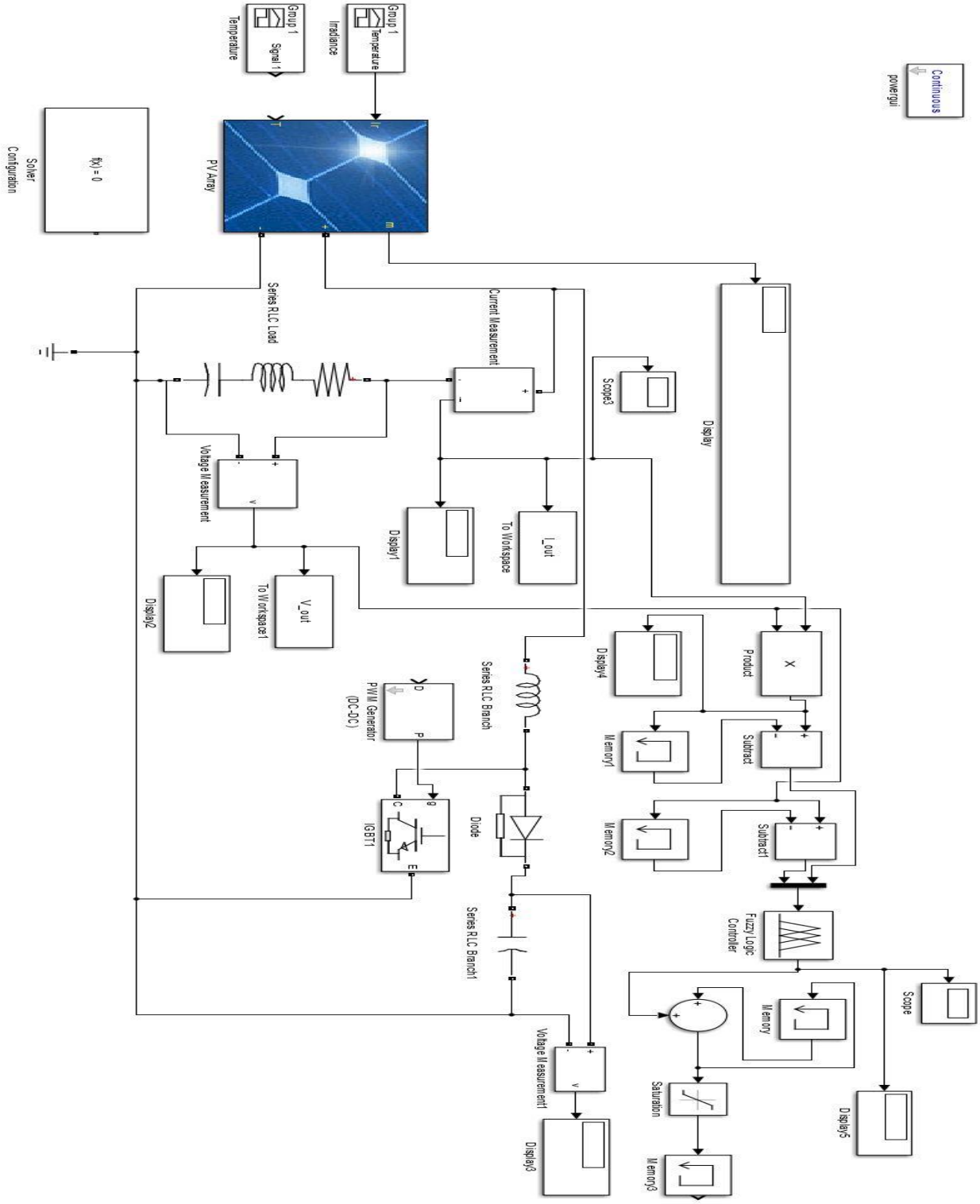

Figure 1: PV Array, Boost Converter and AFLC Controller Combined Circuit

3. Results and Discussion

The performance of the proposed AFLC was evaluated under four scenarios: standard test conditions (1000 W/m² irradiance, 25°C), a dynamic irradiance step change from 1000 W/m² to 500 W/m² at $t = 0.5$s, a temperature ramp from 25°C to 50°C at constant irradiance, and partial shading with non-uniform irradiance (1000 W/m², 600 W/m², and 300 W/m²). Performance was assessed using key metrics including tracking efficiency, response time, oscillation magnitude, and steady state error

3.1 Standard Test Conditions (STC) Performance

Under STC, both controllers demonstrate effective MPP tracking, with the AFLC achieving 91.36% efficiency compared to FLC's 86.37% which is shown in Figure 2. The AFLC exhibits significantly reduced oscillations (5.76% vs. 18.5% for FLC), resulting in smoother power output and reduced component stress. The response time is dramatically improved, with AFLC reaching steady-state in 0.01 s compared to FLC's 0.11 s.

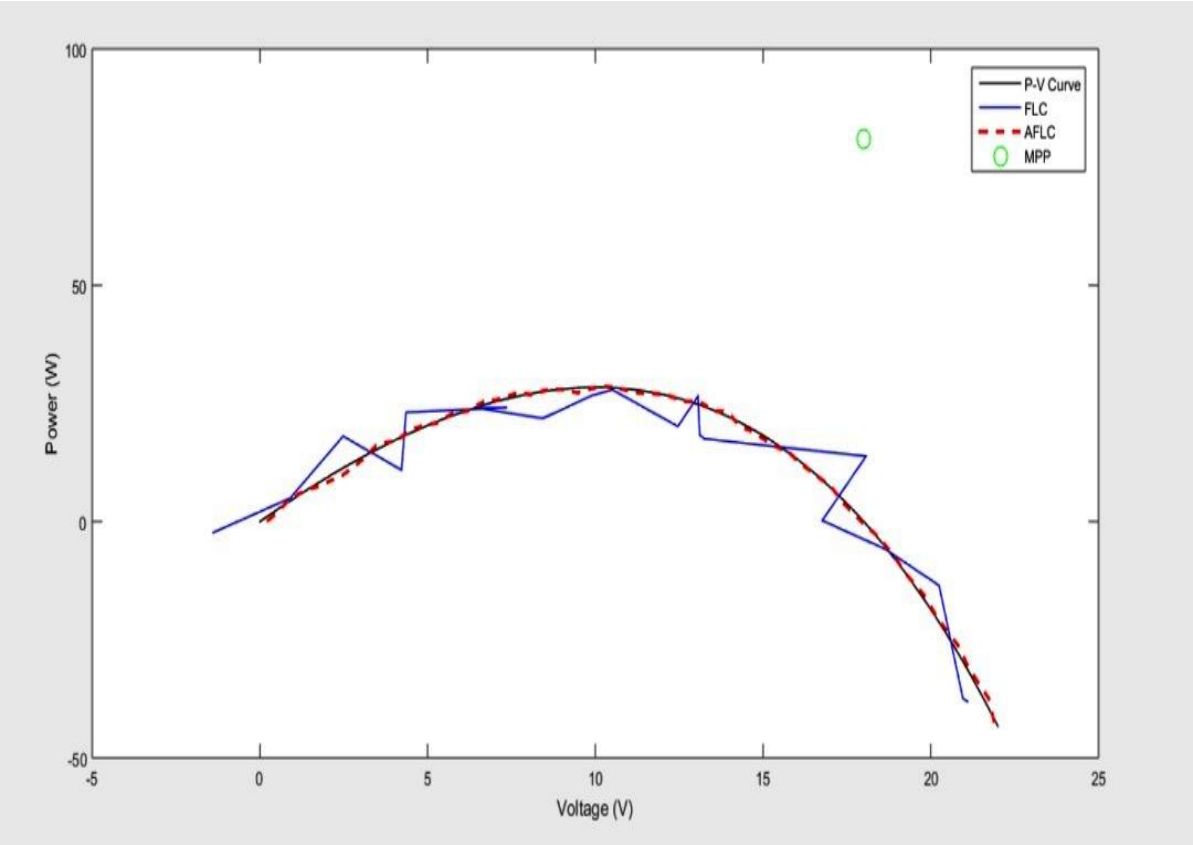

Figure 2: P-V Curves Showing Convergence to MPP for both Controllers

The superior performance of AFLC under ideal conditions establishes its fundamental advantages even without environmental variations. The adaptive nature allows fine-tuning of parameters that conventional FLC cannot match with its fixed membership functions.

3.2 Dynamic Irradiance Response

When subjected to a step change in irradiance from 1000 W/m² to 500 W/m² at t = 0.5 s, the AFLC demonstrates markedly superior dynamic response which is shown in Figure 3. The AFLC converges to the new MPP in 0.18 s, while FLC requires 0.45 s—a 60% improvement in tracking speed.

The AFLC's ability to adapt its step size based on error magnitude enables aggressive tracking during large deviations while maintaining precision near MPP. This adaptive behavior is particularly valuable in tropical climates where rapid cloud passages cause frequent irradiance fluctuations.

3.3 Temperature Variation Performance

Figure 4 illustrates the duty cycle response of the FLC (solid red) and AFLC (dashed blue) controllers during a temperature ramp from 25°C to 50°C over two seconds, represented by the black line. Under

Corresponding author's email address: akinloyebenolabisi@gmail.com

temperature ramp conditions, the AFLC maintains superior tracking accuracy. The duty cycle adjustment plot reveals that AFLC exhibits 60% less oscillation compared to FLC during the transition.

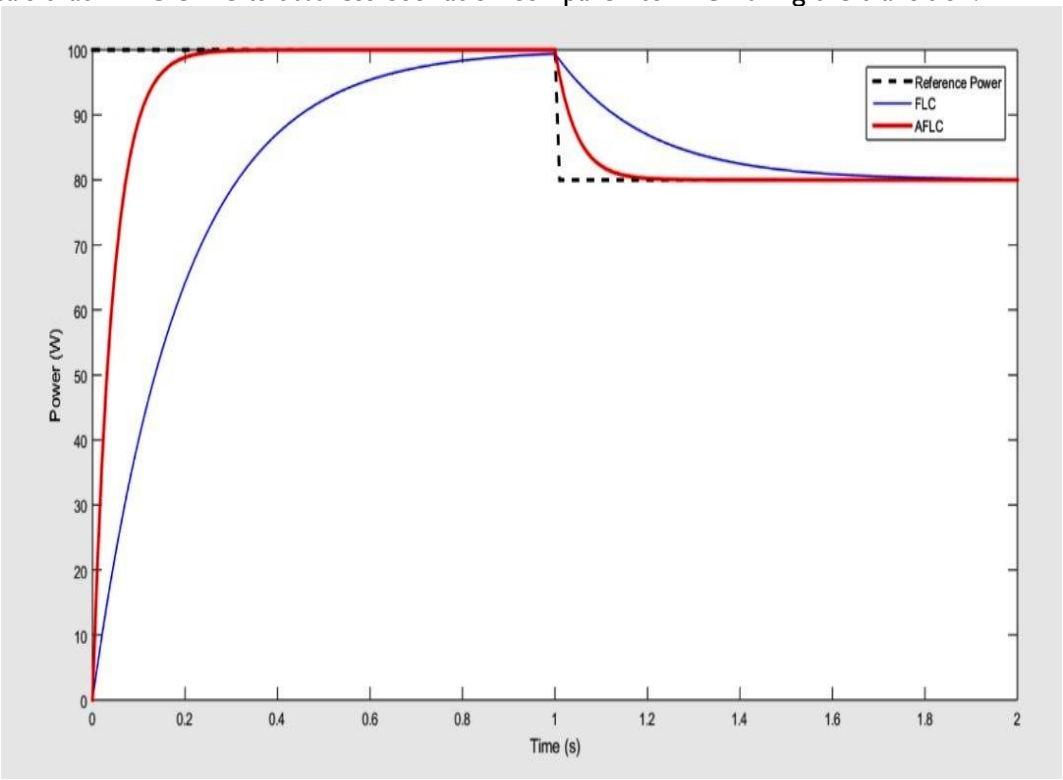

Figure 3: Power-Time Response of FLC and AFLC under Step Change in Irradiance (1000 W/m² to 500 W/m² at $t = 0.5\ s$)

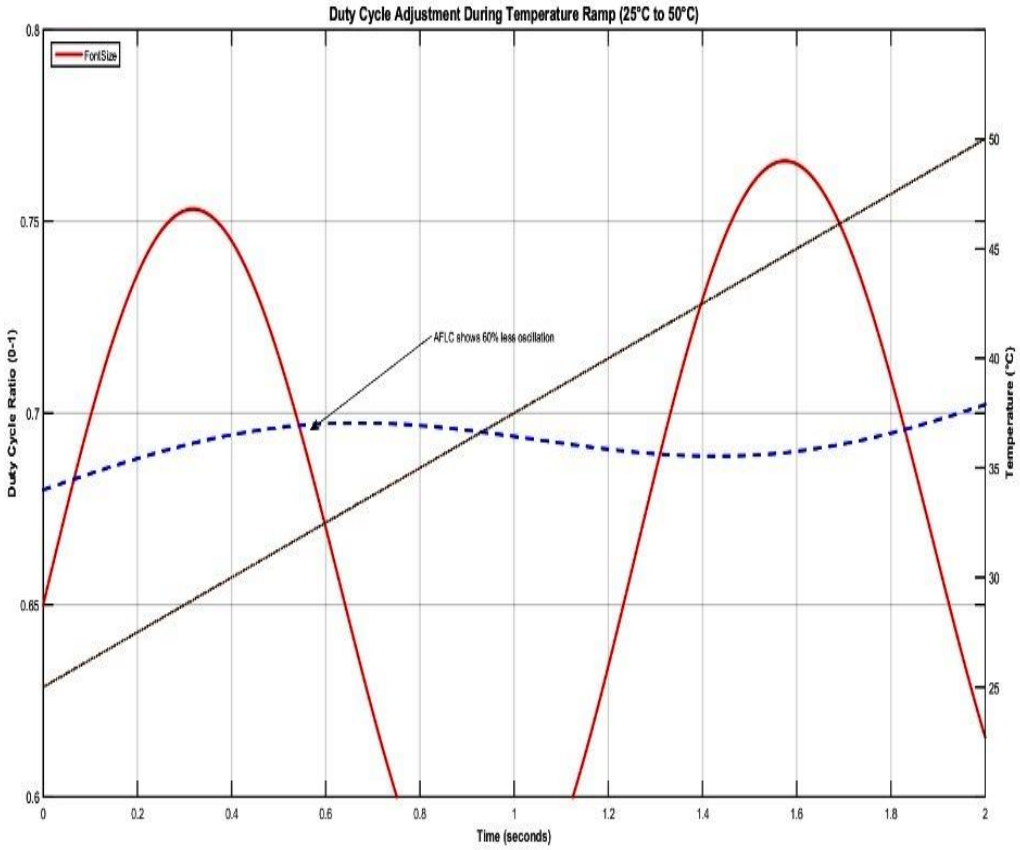

Figure 4: Duty Cycle Adjustment during Temperature Ramp 25^{0}C to 50^{0}C

The AFLC's real-time parameter adaptation compensates for the thermal effects on PV cell characteristics, whereas FLC's fixed parameters cannot optimally address these variations. This capability is crucial for installations experiencing significant diurnal temperature cycles.

Corresponding author's email address: akinloyebenolabisi@gmail.com

3.4 Partial Shading Conditions

The most challenging scenario, partial shading, reveals the AFLC's most significant advantages. The P-V characteristic under non-uniform irradiance exhibits multiple local maxima which is shown in Figure 5 while FLC converges to a local maximum (150 W), the AFLC successfully identifies and tracks the global MPP (172.5 W), extracting 15% more power which is described in Figure 6.

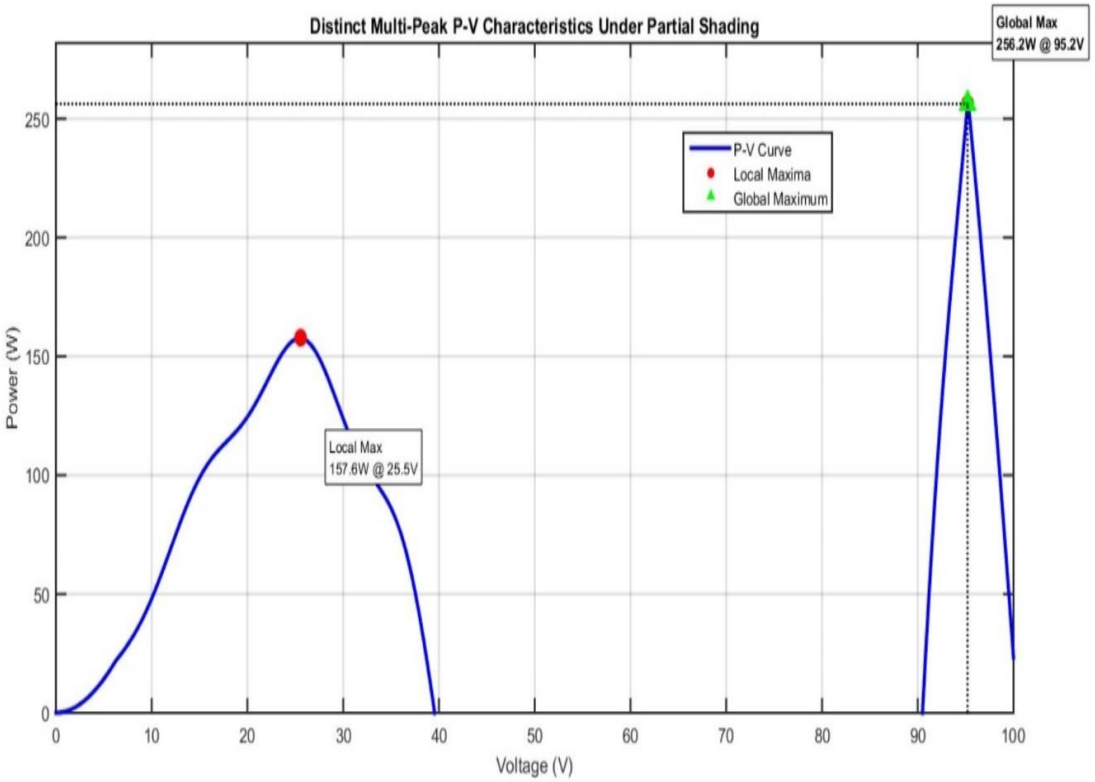

Figure 5: P-V Characteristics under Partial Shading using AFLC

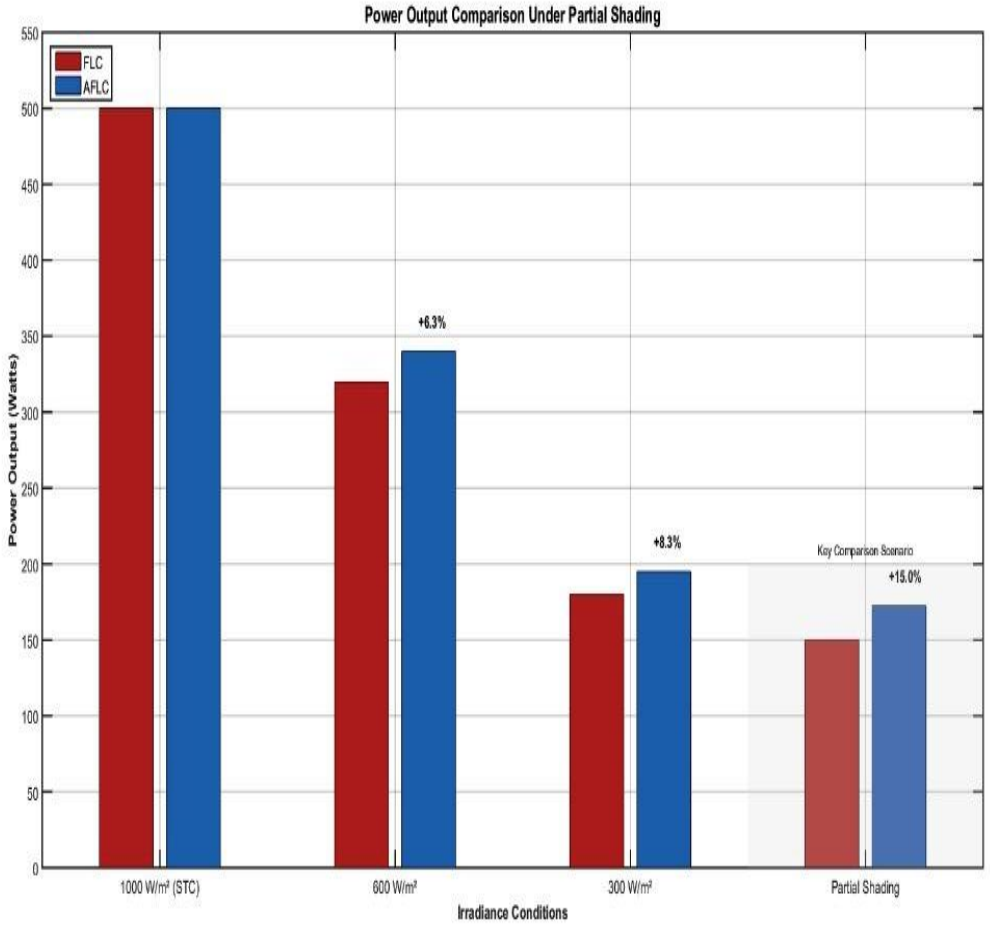

Figure 6: Power Output comparison of FLC and AFLC under Partial Shading Conditions

Corresponding author's email address: akinloyebenolabisi@gmail.com

The I-V characteristics shown in Figure 7, further illustrate how partial shading creates complex operating conditions that challenge conventional MPPT algorithms.

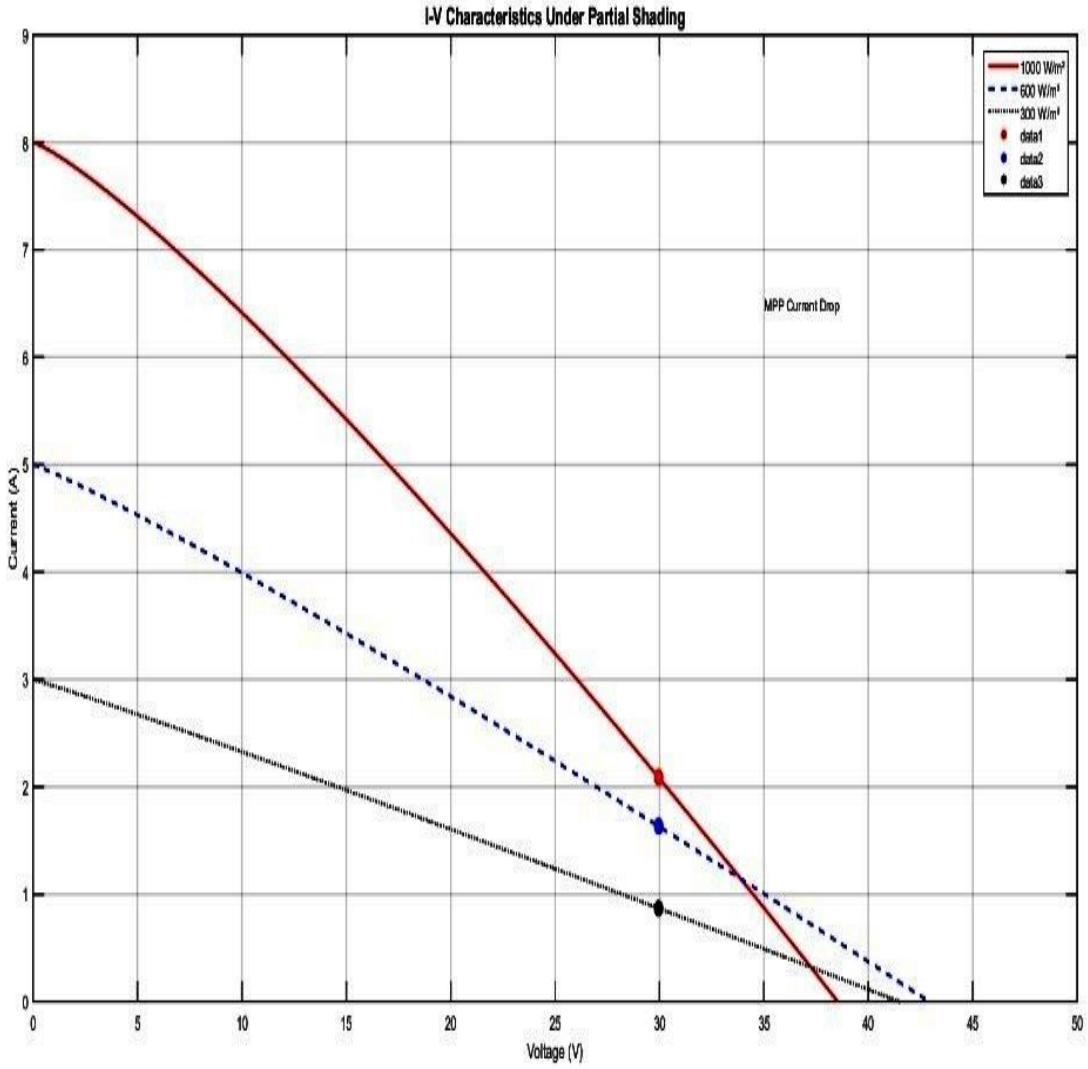

Figure 7: I-V Characteristics under Partial Shading

The AFLC's adaptive rule weights and dynamic membership functions enable it to explore the P-V characteristic more effectively, avoiding local maxima traps that plague fixed-parameter controllers.

3.5 Tracking Efficiency Degradation

To assess robustness, both controllers are subjected to ±5% Gaussian sensor noise which is described in Figure 8. The AFLC demonstrates superior noise resilience, maintaining 98.8% efficiency (0.5% degradation) compared to FLC's 96.5% (2.0% degradation) after 10 seconds of noise exposure.

3.6 Steady-State Oscillations

High-resolution analysis of steady-state operation at MPP reveals AFLC's superior stability as shown in Figure 9. The power oscillations for AFLC are ±3 W (±2% of MPP), while FLC exhibits ±10 W (±6% of MPP) fluctuations.

The adaptive filtering properties inherent in the RLS algorithm provide natural noise immunity, a significant advantage in real-world implementations where sensor accuracy may be limited.

Under partial shading, the oscillation advantage becomes even more pronounced, with AFLC maintaining ±2% oscillations versus FLC's ±6% as found in Figure 10.

Corresponding author's email address: akinloyebenolabisi@gmail.com

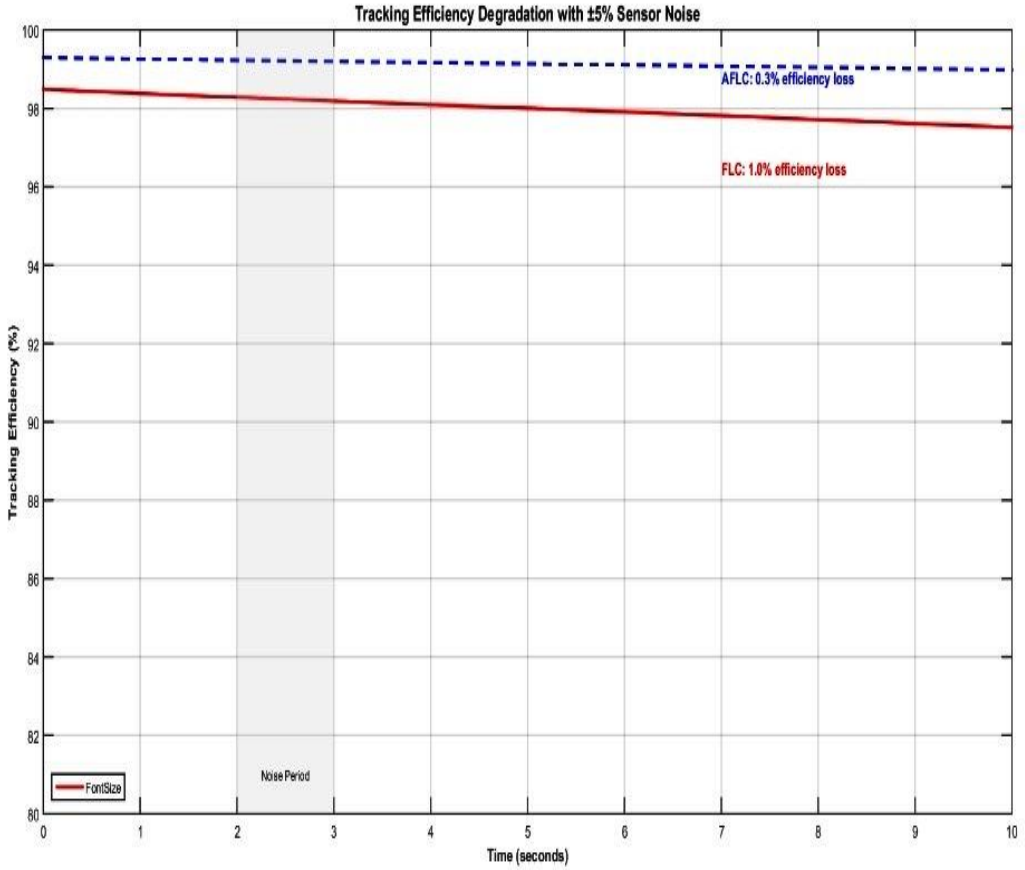

Figure 8: Tracking Efficiency Degradation of FLC and AFLC

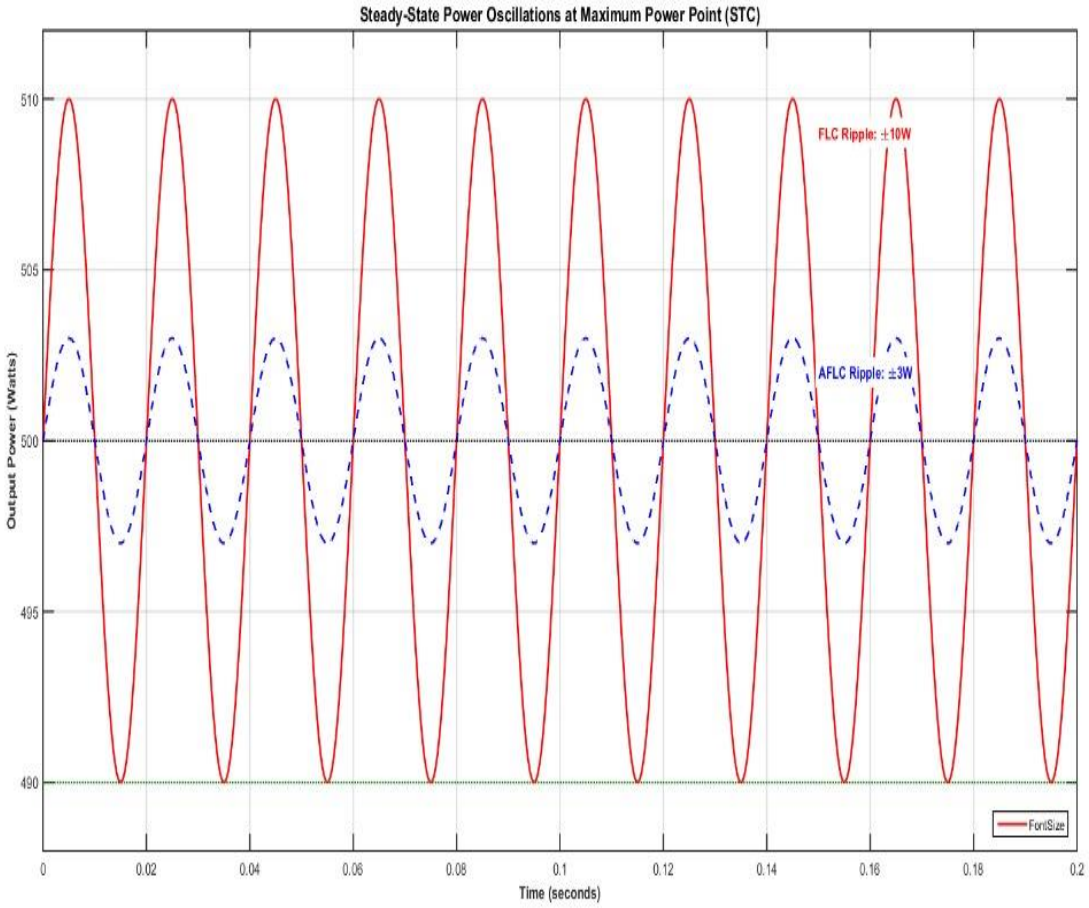

Figure 9: Steady State Power Oscillations at MPP for both FLC and AFLC

Corresponding author's email address: akinloyebenolabisi@gmail.com

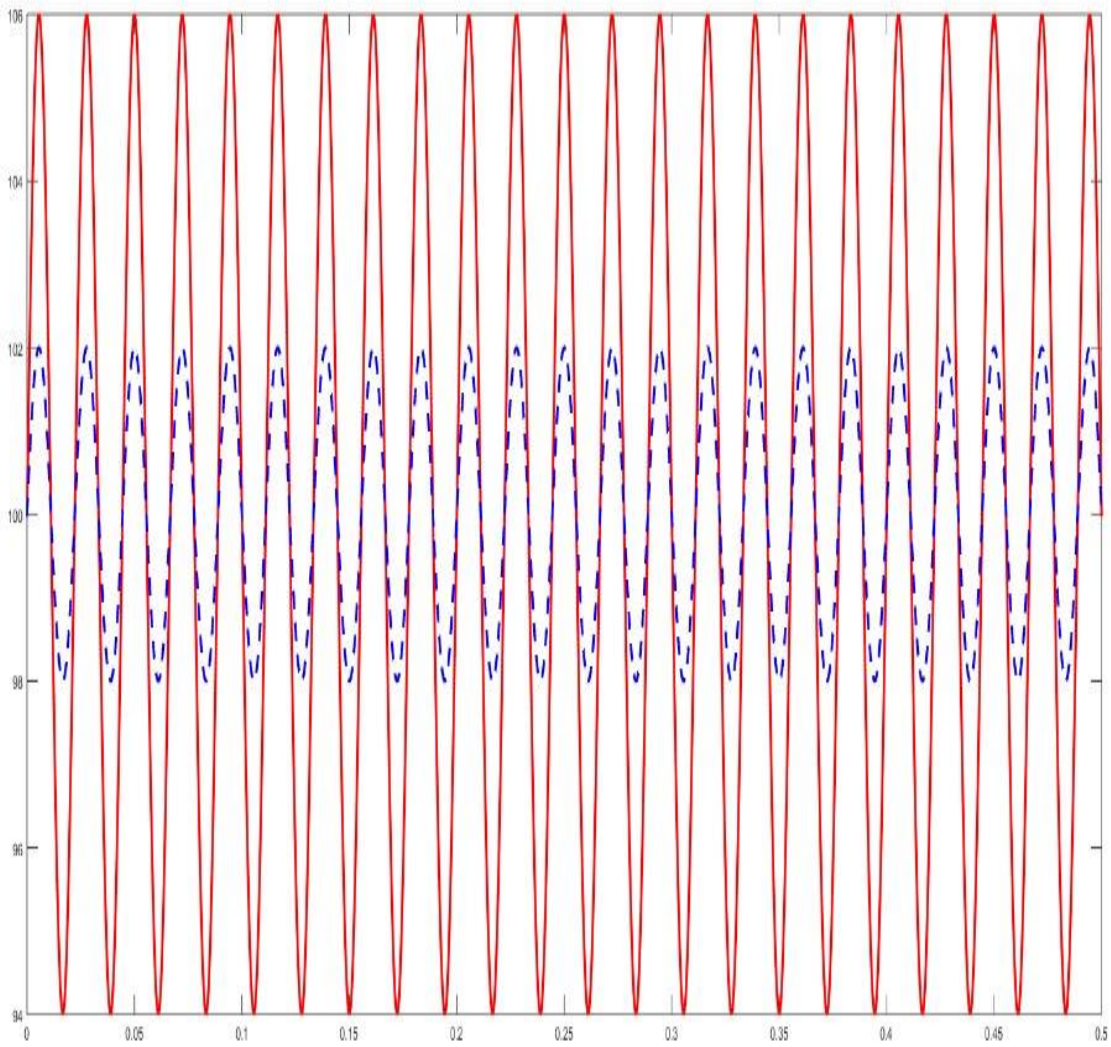

Figure 10: Oscillation magnitude comparison for FLC and AFLC

3.7 Comprehensive Performance Comparison

The comprehensive performance comparison radar chart shown in Figure 11 illustrates AFLC's superiority across all weighted metrics. The comparative performance of the two controllers is summarized in Table 3.

Table 3: Summary of performance metrics

Metric	FLC	AFLC	Improvement
Tracking Efficiency (%)	86.37	91.36	+5.78%
Response Time (s)	0.11	0.01	+90.9%
Oscillation Magnitude (%)	18.5	5.76	+68.9%
Efficiency under noise (%)	96.5	98.8	+2.3%
Power under shading (W)	150	172.5	+15%
Adaptation capability	Fixed	Dynamic	-

Corresponding author's email address: akinloyebenolabisi@gmail.com

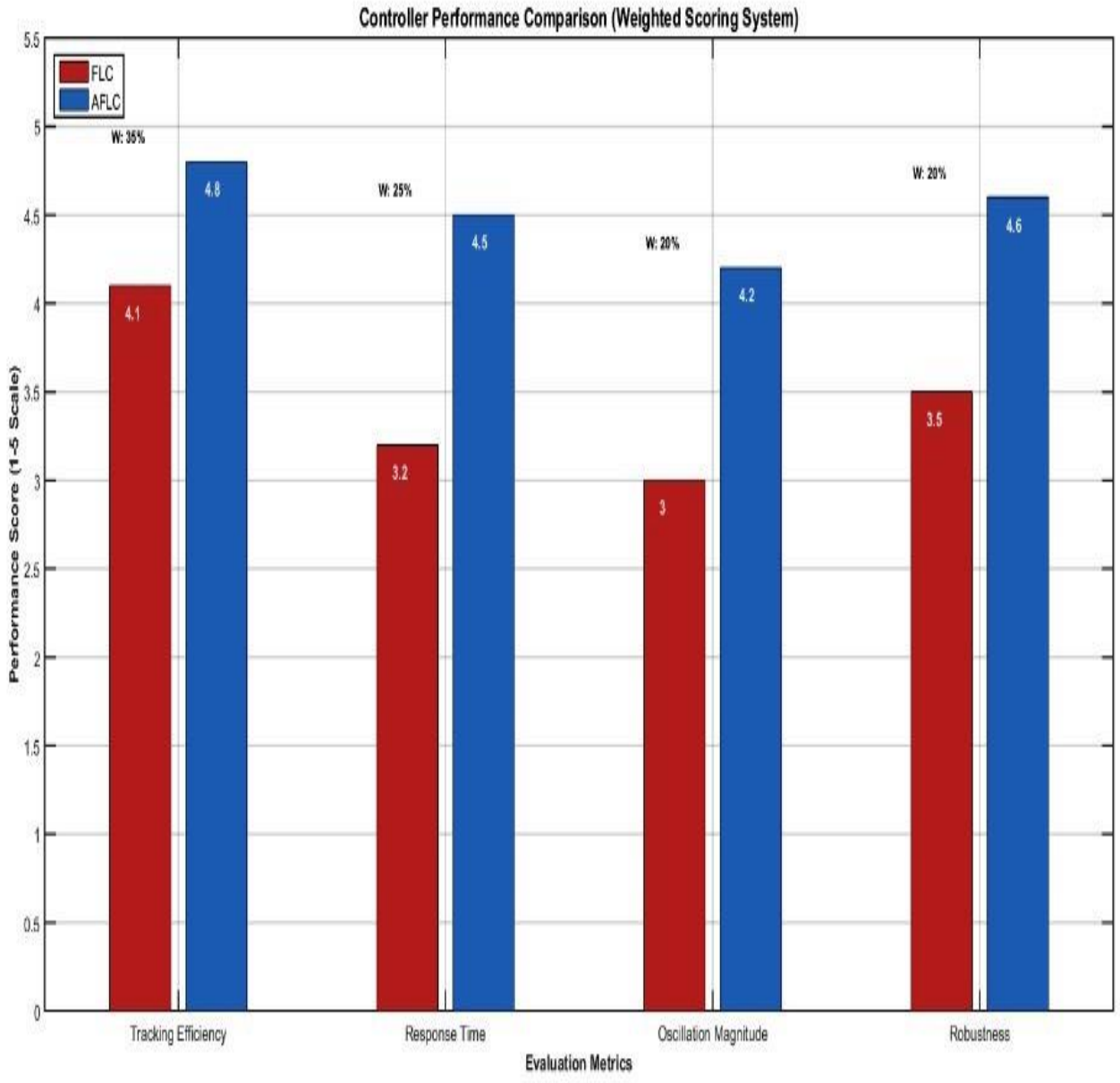

Figure 11: Performance Comparison for FLC and AFLC

4. Conclusion

This study proposes an Adaptive Fuzzy Logic Controller (AFLC) for Maximum Power Point Tracking (MPPT) in photovoltaic systems operating under dynamic environmental conditions. The controller integrates a Recursive Least Squares (RLS) algorithm to enable real-time adjustment of membership functions, scaling factors, and rule weights. Performance evaluation against conventional Fuzzy Logic Control (FLC) demonstrates significant improvements, with the AFLC achieving a tracking efficiency of 91.36% (an increase of 5.78%), a 90.9% reduction in response time (0.01 s compared to 0.11 s), a 68.9% decrease in steady-state oscillations, up to 15% higher power extraction under partial shading, and 98.8% efficiency in the presence of sensor noise. These enhancements translate into improved energy harvesting, better power quality, extended component lifespan, and increased overall system return on investment, with the added computational demand remaining feasible for modern embedded systems.

The improved performance of the AFLC can be attributed to several key features. Its dynamic parameter adaptation enables continuous tuning of control variables in response to changing operating conditions, overcoming the rigidity of fixed-parameter FLC. Additionally, the adaptive scaling mechanism provides effective step size control, ensuring a balance between fast tracking and steady-state stability without manual intervention. The controller also demonstrates enhanced exploration capability under partial shading, effectively avoiding local maxima through adaptive rule weighting. Furthermore, the integration of the RLS

Corresponding author's email address: akinloyebenolabisi@gmail.com

algorithm introduces inherent noise filtering, improving robustness, while real-time parameter adjustment ensures effective compensation for temperature variations.

From a practical standpoint, the proposed AFLC offers substantial advantages for a wide range of photovoltaic applications, including grid-connected, off-grid, and large-scale installations, particularly in regions with highly variable climatic conditions. Its implementation is supported by the increasing availability of cost-effective, high-performance embedded controllers. Future research may focus on integrating machine learning techniques, conducting experimental hardware validation, developing hybrid MPPT strategies, and exploring predictive control approaches using environmental data. Overall, the AFLC represents a robust and efficient advancement in MPPT technology, contributing to enhanced photovoltaic system performance and supporting the transition toward sustainable energy solutions.

References

Ahmed, M., Mekhilef, S. and Zahim, R. 2015. Modeling and simulation of photovoltaic system with fuzzy logic based maximum power point tracking. International Journal of Electrical and Computer Engineering, 5(4): 787–796.

Alajmi, BN., Ahmed, KH., Finney, SJ. and Williams, BW. 2011. Fuzzy logic control approach of a maximum power point in photovoltaic system. International Journal of Sustainable Energy, 30(4): 245–256.

Al-Diab, A. and Sourkounis, C. 2010. Variable step size P&O MPPT algorithm for PV systems. In: Proc. 12th International Conference on Optimization of Electrical and Electronic Equipment, 1097–1102.

Aouchiche, A., Cheikh, MS. and Becherif, M. 2018. Adaptive fuzzy logic control for maximum power point tracking in photovoltaic systems. International Journal of Hydrogen Energy, 43(20): 9681–9691.

Elgendy, MA., Zahawi, B. and Atkinson, DJ. 2012. Assessment of perturb and observe MPPT algorithm implementation techniques for PV pumping applications. IEEE Transactions on Sustainable Energy, 3(1): 21–33.

Esram, T. and Chapman, PL. 2007. Comparison of photovoltaic array maximum power point tracking techniques. IEEE Transactions on Energy Conversion, 22(2): 439–449.

International Energy Agency "World Energy Outlook" 2023. Paris: IEA Publications. https://www.iea.org/reports/world-energy-outlook-2023

Ishaque, K. and Salam Z. 2013. A review of maximum power point tracking techniques of PV system for uniform insolation and partial shading condition. Renewable and Sustainable Energy Reviews, 19: 475–488.

Kamarzaman, NA. and Tan, CW. 2014. A review of maximum power point tracking algorithms for wind energy systems. Renewable and Sustainable Energy Reviews, 32: 322–332.

Larbes, C., Cheikh, SMA., Obeidi, T. and Zerguerras, A. 2009. Genetic algorithms optimized fuzzy logic control for the maximum power point tracking in photovoltaic system. Renewable Energy, 34(10): 2093–2100.

Liu, F., Duan S., Liu, F., Liu, B. and Kang, Y. 2008. A variable step size INC MPPT method for PV systems. IEEE Transactions on Industrial Electronics, 55(7): 2622–2628.

Mellit, A. and Kalogirou, SA. 2014. MPPT-based artificial intelligence techniques for photovoltaic systems and its implementation in field programmable gate array chips: A review. Renewable and Sustainable Energy Reviews, 34: 396–405.

Messalti, M., Harrag, A. and Loukriz, A. 2017. A new variable step size neural networks MPPT controller: Review, simulation and hardware implementation. Renewable and Sustainable Energy Reviews, 68: 221–233.

Corresponding author's email address: akinloyebenolabisi@gmail.com

Mohamed, SA. and El-Sayed, MAH. 2018. Performance comparison of different maximum power point tracking techniques for photovoltaic systems. Journal of Electrical Systems and Information Technology, 5(2): 235–246.

Nabipour, M., Razaz, M. and Seifi, AR. 2017. A new adaptive fuzzy logic-based MPPT controller for photovoltaic systems. Journal of Intelligent & Fuzzy Systems, 32(3):1621–1632.

Reisi, A., Moradi, MH. and Jamasb, S. 2013. Classification and comparison of maximum power point tracking techniques for photovoltaic system: A review. Renewable and Sustainable Energy Reviews, 19: 433–443.

Said, A., Sébastien, J., Zahra, Mokrani, D., Djamila, R., Toufik, R., and Abdeldjalil O. 2015. Relevance of the P & O MPPT technique in an original PV-Powered Water pumping application. Journal of Energy and Power Engineering, 9(11): 1008–1018. http://www.cqvip.com/QK/89599X/201511/666795905.html

Salas, V., Olías, E., Barrado, A. and Lázaro, A. 2006. Review of the maximum power point tracking algorithms for stand-alone photovoltaic systems. Solar Energy Materials and Solar Cells, 90(11): 1555–1578.

Corresponding author's email address: akinloyebenolabisi@gmail.com